Journal of Asian Earth Sciences 65 (2013) 100–106

Contents lists available at SciVerse ScienceDirect

Journal of Asian Earth Sciences

journal homepage: www.elsevier.com/locate/jseaes

A preliminary seismic study of Taal Volcano, Luzon Island Philippines

S.-H. You [a], Y. Gung [a,*], C.-H. Lin [b], K.I. Konstantinou [c], T.-M. Chang [d], E.T.Y. Chang [e], R. Solidum [f]

[a] Department of Geosciences, National Taiwan University, Taipei, Taiwan
[b] Institute of Earth Sciences, Academia Sinica, Taipei, Taiwan
[c] Department of Earth Sciences, National Central University, Taoyuan, Taiwan
[d] National Center for Research on Earthquake Engineering, Taipei, Taiwan
[e] Institute of Oceanography, National Taiwan University, Taipei, Taiwan
[f] Philippine Institute of Volcanology and Sesimology, Quezon, Philippines

ARTICLE INFO

Article history:
Available online 7 November 2012

Keywords:
Taal Volcano
Seismicity
1-D velocity model
Noise cross-correlation

ABSTRACT

The very active Taal Volcano lies in the southern part of Luzon Island only 60 km from Manila, the capital of the Philippines. In March 2008 we deployed a temporary seismic network around Taal that consisted of 8 three-component short period seismometers. This network recorded during the period from March to November 2008 about 1050 local events. In the early data processing stages, unexpected linear drifting of clock time was clearly identified for a number of stations. The drifting rates of each problematic station were determined and the errors were corrected before further processing. Initial location of each event was derived by manually picked P-/S-phases arrival times using HYPO71 and a general velocity model based on AK135. Since the velocity structure beneath Taal is essentially unknown, we used travel times of 338 well-located events in order to derive a minimum 1D velocity model using VELEST. The resulting locations show that most events occurred at the shallow depth beneath the Taal Volcano, and two major earthquake groups were noticed, with one lying underneath the western shore of Taal lake and the other one spread around the eastern flank of the Taal Volcano. Since there is no reported volcano activities during the operation period of our seismic array, we are still not confident to interpret these findings in terms of other natures of volcano at the current stage. However, our work represents an important pioneer step towards other more advanced seismic studies in Taal Volcano.

1. Introduction

Taal Caldera (~20 × 30 km) is located 60 km south of Metro Manila on Luzon Island. Inside the caldera is Taal Lake, and Taal Volcano Island is located at the center of the lake. The Taal Volcano Island is a ~5 km diameter post-caldera structure composed of several eruption centers. Taal Volcano is a 311-m-high stratovolcano with a lake (Main Crater Lake, 1.2 km wide and 75 m deep) filling the central crater.

Taal Volcano is one of the 15 most dangerous "Decade Volcanoes" that represent especially high potential hazards to nearby population centers (e.g., Zlotnicki et al., 2009). At least 33 eruptions were recorded since its first documented activity in 1572, among which the most well-known one is the eruption that occurred in 1965. During this VEI 4 event, pyroclastic surges that originated from the southwest flank of the island killed about 200 people (Moore et al., 1966).

The subsurface plumbing activities beneath the volcanic area are manifested through various geochemical and geothermal observations, and are usually accompanied by earthquakes. Activities of Taal Volcano have been attentively monitored by the Philippine Institute of Volcanology and Seismology (PHIVOLCS). In the early 90s, three seismic swarms were reported in Taal area: in early 1991, in February 1992 and March 1994. The February 1992 activity was accompanied by a rapid ground deformation at a rate of about 10–20 cm uplift in a day, and active fissures opened along the E–W northern flank during the 1992–1994 seismic activity. Thus, it has been considered to be in a possible state of unrest since 1994, as seen from seismic swarms, ground deformation, geysering activity and changes in temperature and chemistry (http://www.phivolcs.dost.gov.ph). Studies based on GPS data from 1998–1999 indicate that the largest deformation correlates in time with anomalous bursts of hydrothermal activity and high-frequency local seismicity, suggesting that both deformation and seismicity are responding to migration of hydrothermal fluids (Bartel et al., 2003). More recently, seismicity in Taal Volcano increased from September 2004. A seismic swarm with a maximum of 20 events in a day was recorded on 13 February 2005. After February 2005, seismicity slowly decreased until new record of seismic swarms in December 2005. Results from multidisciplinary observations combining electromagnetic, geochemical and thermal

* Corresponding author.
E-mail address: ycgung@ntu.edu.tw (Y. Gung).

1367-9120/$ - see front matter © 2012 Elsevier Ltd. All rights reserved.
http://dx.doi.org/10.1016/j.jseaes.2012.10.027

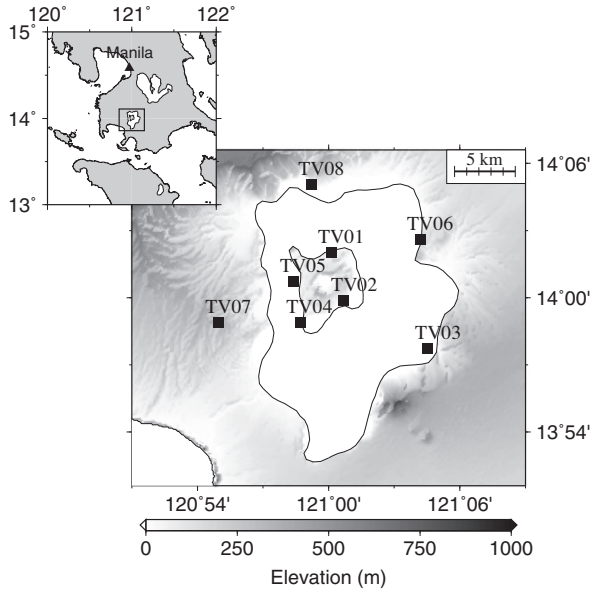

Fig. 1. Station locations (shown here by solid squares) of Taal seismic array. The small box in the upper-left panel shows the study region, in which Manila city is also shown by a solid triangle.

Table 1
Station information of Taal seismic Array.

Station	Longitude	Latitude	Elevation (m)	Deployed time
TV01	121.0020	14.0341	19	2008/03/25
TV02	121.0117	13.9979	27	2008/03/25
TV03	121.0756	13.9621	11	2008/03/25
TV04	120.9784	13.9813	40	2008/03/26
TV05	120.9729	14.0121	14	2008/03/26
TV06	121.0700	14.0435	137	2008/03/26
TV07	120.9161	13.9814	321	2008/03/26
TV08	120.9867	14.0843	19	2008/07/21

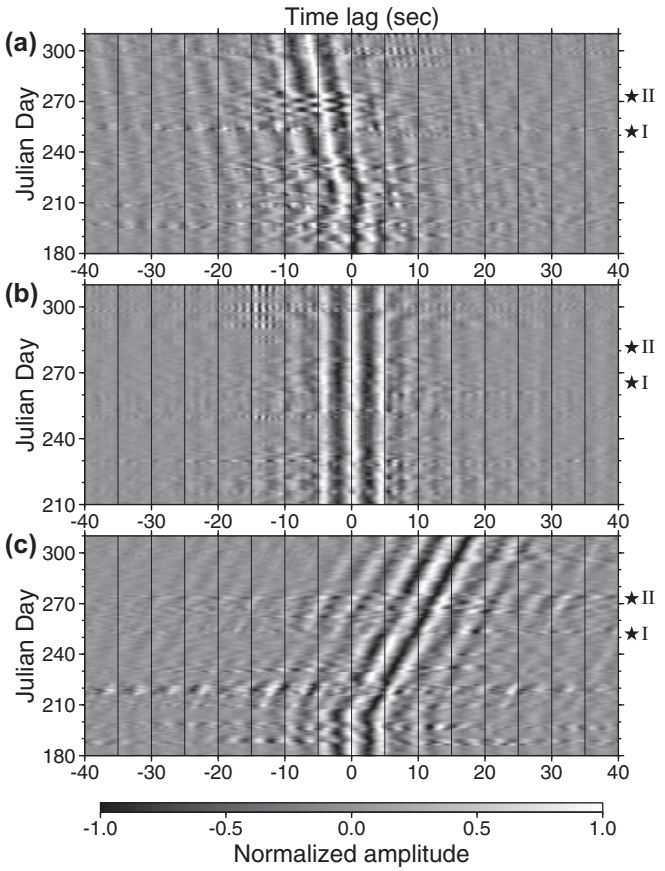

Fig. 2. Examples for clock errors revealed by noise CCFs. Daily CCFs of pairs TV04–TV02 (a), TV05–TV04 (b), and TV06–TV04 (c) are presented here. The waveform of CCFs is shown in terms of scaled gray pixel with amplitudes normalized individually. The symmetric centers of CCF pairs in (a) and (c) clearly drift away from the zero time lag. The star symbols on the right side of each panel mark the occurring time of teleseismic events discussed in Fig. 3, with "I" for event 2008/09/08 (Fig. 3b), and "II" for event 2008/09/29 (Fig. 3c).

survey, suggest that the northern flank located between the crater rim and the 1992–1994 fissures is connected with a deep thermal source in Main crater and is reactivated during seismic activity (Zlotnicki et al., 2009).

Various seismological approaches have been used in volcano studies. Analysis of seismicity and seismic tomography can provide information about structure and evolution of magma chambers (e.g. Sherburn et al., 1998; Tanaka et al., 2002; Konstantinou et al., 2007), which may even be used to forecast volcanic eruptions (e.g. Harlow et al., 1996; Bryan and Sherburn, 1999; Jones et al., 2001). Properties of long period (LP) seismic signals, characterized by single or multiple impulse-like excitations in the frequency domain can be used to infer the status of volcanoes (e.g. Chouet, 1996; McNutt, 1996; Kumagai et al., 2002). Lately, it has been shown that the Green's function of elastic waves between two seismic stations resembles the cross-correlation functions (CCFs) of their noisy continuous records (e.g., Weaver and Lobkis 2001, 2002; Shapiro and Campillo, 2004; Snieder, 2004). Structure perturbations induced by volcanic activities can thus have an impact on the noise-derived empirical Green's functions (EGFs). The idea has been applied to the detection of the subsurface magma activities by examining the robust coda train tailing the major signal of EGFs (Brenguier et al., 2008).

Given the well documented active seismicity in Taal Volcano, no further seismic investigations have been employed in this area, since there was no local seismic network deployed until late March 2008.

In this study, with local earthquakes recorded by the newly deployed seismic network, we aim to construct the first 1-D model of seismic velocities for the area around Taal Volcano. A reliable 1-D model is a precondition for most other seismic studies, such as 3-D tomography or more accurate determination of locations of earthquake hypocenters. On the other hand, in a parallel project using the same data set, we also examine the temporal variations of noise-derived EGFs, to explore the potential subsurface perturbations induced by volcanic activities, and to ensure the timing quality of the seismic data. Unexpected linear time-drifting of internal clock were noticed from noise-derived daily CCFs. The clock errors have been further confirmed by teleseismic signals, and were corrected before further data processing for the development of the 1-D model.

2. Temporary seismic array

To investigate seismicity and structure beneath the Taal Caldera, we deployed a temporary seismic array consisting of seven stations (TV01–TV07) in late March 2008. Four of them were deployed on the Taal Volcano Island, the other three on lakeshore around the Taal Lake. On 21 July 2008, one more station (TV08) was added in northern lakeshore, near the PHIVOLCS observatory. Each station is equipped with a short-period three-component seismometer (Lennartz Electronic LE-3D Lite 1 Hz) and a GPS synchronized clock. The data are continuously recorded and sampled

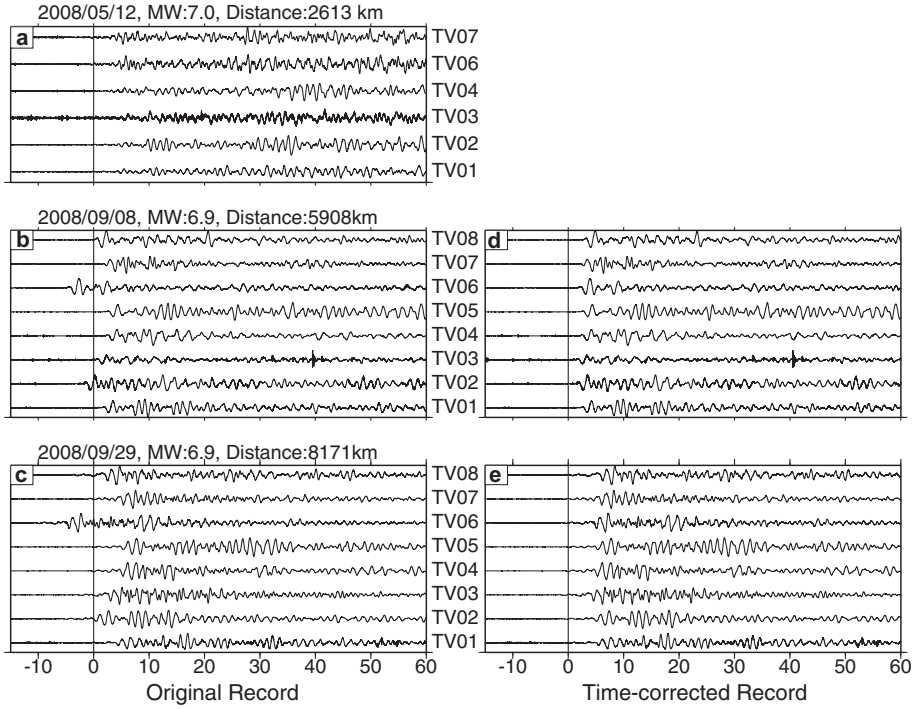

Fig. 3. The vertical component waveform of three teleseismic events recorded by the Taal array. (a): 2008/05/12, 06:28:01.57, 31.002°N, 103.322°E, depth: 36 km, MW7.0, Sichuan, China. (b): 2008/09/08, 18:52:06.97, 13.401°S, 166.967°N, depth: 110 km, MW 6.9, Vanuatu Islands. (c) 2008/09/29, 15:19:31.59, 29.756°S, 177.683°W, depth: 35 km, MW: 6.9, Kermadec Islands, New Zealand. The black line in each panel represents the predicted P arrival time for the central location of array from each event. In both events (b) and (c) the accumulated timing errors in TV02 and TV06 are evident. Records shown in panels (d) and (e) are time-corrected results for event (b) and (c) respectively.

Table 2
Time-drifting rates determined by linear regression. T is the predicted drifting time, T_0 the time in the data record and ΔD the number of drifting days. The standard deviations (the number behind ±) for each station are also shown.

Station	Time-drifting trend
TV01	$T = T_0 - 0.015 \times \Delta D \pm 0.015$
TV02	$T = T_0 - 0.068 \times \Delta D \pm 0.063$
TV03	$T = T_0 - 0.022 \times \Delta D \pm 0.015$
TV06	$T = T_0 - 0.140 \times \Delta D \pm 0.015$
TV07	$T = T_0 - 0.010 \times \Delta D \pm 0.018$
TV08	$T = T_0 - 0.053 \times \Delta D \pm 0.050$

at 100 Hz with a digital recorder (Tokyo Sokushin digital recorder SAMTAC-801H) in all stations. The locations and relevant information of the seismic array are presented in Fig. 1 and Table 1.

3. Timing errors

Data recorded from late March 2008 to early November 2008 are used in this study. Besides the event identification and phase picking for the development of a seismic model, the continuous data of the same time period has also been used in a separate study, in which we examine the CCFs derived by continuous 1-bit data (e.g., Shapiro and Campillo, 2004) of station pairs, aiming to explore the temporal variations in EGFs which are possibly related to the crust perturbation induced by volcanic activities.

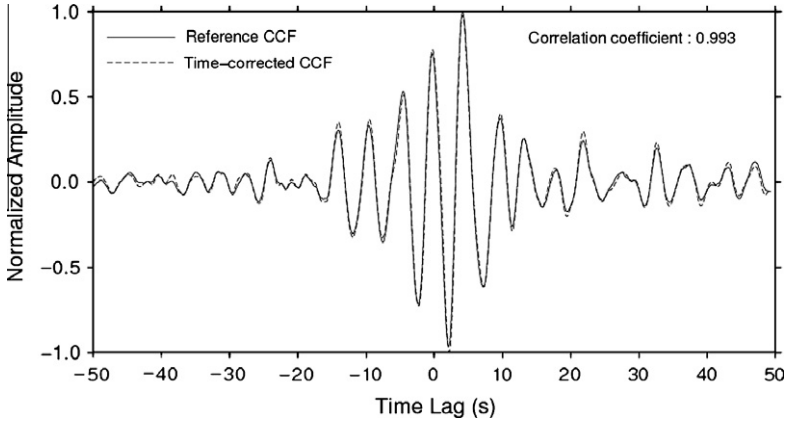

Fig. 4. Comparison of the reference CCF (solid line) and the stacking of time-corrected CCFs for station pair TV06–TV04. The correlation coefficient (0.993) between two traces is also shown in the upper-right corner.

Table 3
The 14-layer initial velocity model.

Depth (km)	Vp (km/s)	Vs (km/s)
−1.0	3.80	2.20
2.0	4.30	2.51
4.0	4.80	2.83
6.0	5.30	3.14
8.0	5.80	3.46
10.0	5.91	3.52
12.0	6.03	3.59
14.0	6.14	3.65
16.0	6.26	3.72
18.0	6.38	3.78
20.0	6.50	3.85
25.0	7.01	4.06
30.0	7.53	4.27
35.0	8.04	4.48

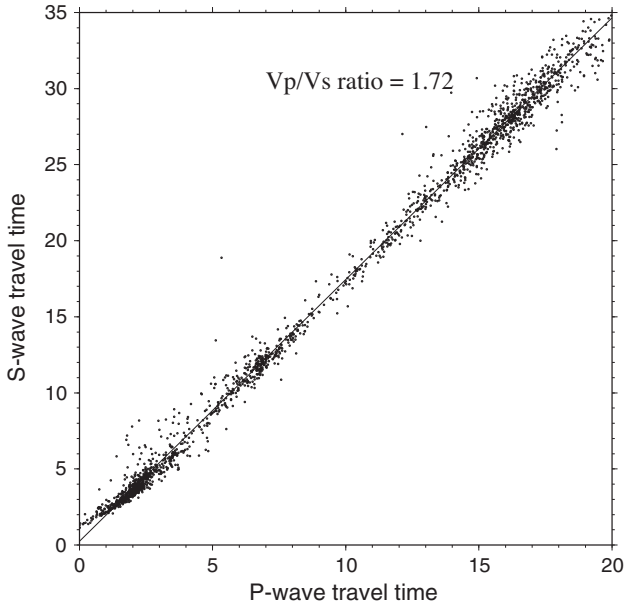

Fig. 5. The Wadati diagram based on results of HYPO71. A regional Vp/Vs ratio of 1.72 is determined from the least square linear fitting for P-wave versus S-wave travel times.

Moreover, the examination of noise-derived EGFs may help to ensure the data quality. Basically, two types of instrument errors can be identified from the noise-derived EGFs: the polarity reversal and time shift of the internal clock. The former is characterized by the reverse phase in waveform as compared to the reference CCFs with correct polarity and the later is accompanied by a time shift of the symmetry between causal (time positive portion of CCF) and acausal (time negative portion of CCF) signals (e.g., You et al., 2010; Lukac et al., 2009).

During the inspection of the noise-derived CCFs, non-negligible time drift of internal clocks of some stations is noticed. Two examples are shown in Fig. 2, in which daily CCFs are aligned for the entire time period, and their amplitudes are normalized to emphasize the gradual shifting of symmetric center. The seemingly linear time-drift in station pair TV04–TV02 (Fig. 2a) and TV06–TV04 (Fig. 2c) are unambiguously due to the timing errors of internal clock. The errors could be introduced by one or both stations of the problematic station pair. To resolve the issue, we first look for reference stations which suffer no such error, as the pair TV04–TV05 shown in Fig. 2b, and compare other CCFs paired by one reference station and one suspected station. Results from Fig. 2a–c thus suggest station TV02 and TV06 are the ones with clock error among the four stations shown here.

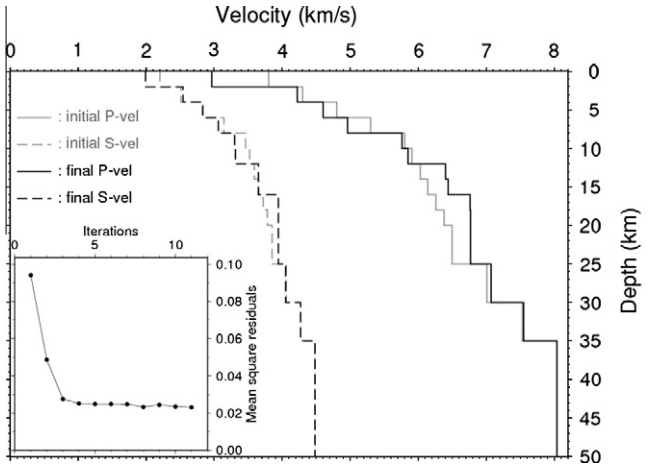

Fig. 6. 14-Layer 1-D models (black lines) of Vp and Vs determined by VELEST. The starting models are shown in gray lines. The result suggests that velocity boundaries at 10 km, 14 km, 18 km and 20 km are not necessary, and there is only minor adjustment for depth below 25 km. The mean square residual for each iteration is shown in the lower-left panel.

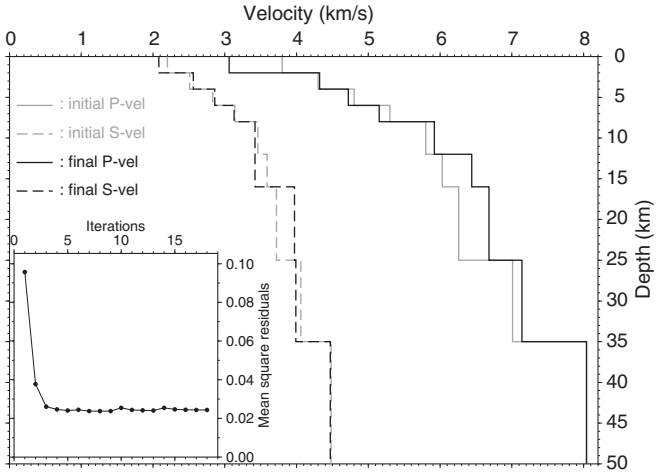

Fig. 7. 9-Layer 1-D models (black lines) of Vp and Vs determined by VELEST. The starting models are shown in gray lines. The mean square residual for each iteration is shown in the lower-left panel.

From the above results and station maintenance log, we conclude that the clock malfunction started on the day after the station maintenance, i.e., July 21–23, 2008. However, the exact cause of time drifting remains unknown.

To further verify the clock errors, we examine earthquake signals from teleseismic events (Fig. 3). The first event occurred on May 12, 2008 (Fig. 3a), time before the clock malfunction began, and the comparison of P-wave arrival time of each station shows no anomalous feature. The second event occurred on September 9, 2008 (Fig. 3b), and the third on September 29, 2008 (Fig. 3c). In both events, the accumulated timing errors in the fore-mentioned TV02 and TV06 are obvious, and the comparison also demonstrate other stations, such as TV03 and TV08, may have similar problem.

The timing errors are apparently too large to be ignored, and proper correction needs to be done before further data processing. To evaluate the time-drifting of each station, stackings of CCFs from the data of the first month are used as reference CCF, for the fact that no clock error was observed in that period as seen from daily CCFs. We then cross-correlate other daily CCFs and their

Table 4
The 9-layer initial velocity model.

Depth (km)	Vp (km/s)	Vs (km/s)
−1.0	3.80	2.20
2.0	4.30	2.51
4.0	4.80	2.83
6.0	5.30	3.14
8.0	5.80	3.46
12.0	6.03	3.59
16.0	6.26	3.72
25.0	7.01	4.06
35.0	8.04	4.48

Table 5
Final velocity determined by VELEST.

Depth (km)	Vp (km/s)	Vs (km/s)
−1.0	3.06	2.08
2.0	4.32	2.56
4.0	4.72	2.86
6.0	5.15	3.13
8.0	5.92	3.42
12.0	6.44	3.42
16.0	6.68	3.97
25.0	7.14	3.99
35.0	8.04	4.47

reference CCFs in the frequency range from 0.2 Hz to 0.5 Hz. The selected frequency band is based on the effective energy distribution of the CCFs amplitude spectrum. The results suggest that all the time-drifting appear to be linear. We thus inverted for the drifting rate of each station using least squares linear regression. The drifting rates and the corresponding standard deviations for each estimate are listed in Table 2. The standard deviations range from 0.015 to 0.063 s, which are small enough for the purpose of this study.

To further assess the accuracy of the time correction scheme, we examine the time-corrected teleseismic signals and CCFs. As is clearly demonstrated (Fig. 3d and e) that the teleseismic arrivals are consistent with each other after time corrections. For the time-corrected CCFs, we compare their stacking with the reference CCF in Fig. 4, where both waveforms are almost identical, and a very high correlation (0.993) between them is achieved. Thus, we have confirmed that the derived drifting rates are reliable. The clock errors of each station are adjusted accordingly prior to the inversion.

4. Minimum 1-D velocity model

Three P arrival pickings is the minimum requirement for the determination of hypocenters using HYPO71 (Lee and Lahr, 1972). For the time period considered, 1050 recorded events are qualified and their first arrivals of P and S waves are manually picked. First, initial locations of these events were determined by HYPO71 with a 14-layer starting model (Table 3). The thickness of each layer is 2 km in the top 20 km, and 5 km in the depth range from 20 to 35 km, below which velocities of uppermost AK135 (Kennett et al., 1995) is used as a half space layer. The model is based on global continental average of AK135, from which velocities at each layer are linearly interpolated with 3.8 km/s for P and 2.2 km/s on the surface layer. Although we aim to build a simpler 1-D model, many thin layers are used in the starting model, as there is no a priori information about how to set up the proper boundary depth for velocity profile. Depending on the results of the 1-D model inversion, layers with similar velocities will be merged.

In the first run of HYPO71, the Vp/Vs ration 1.73 is used. With the derived initial locations, the Vp/Vs ratio 1.72 is then

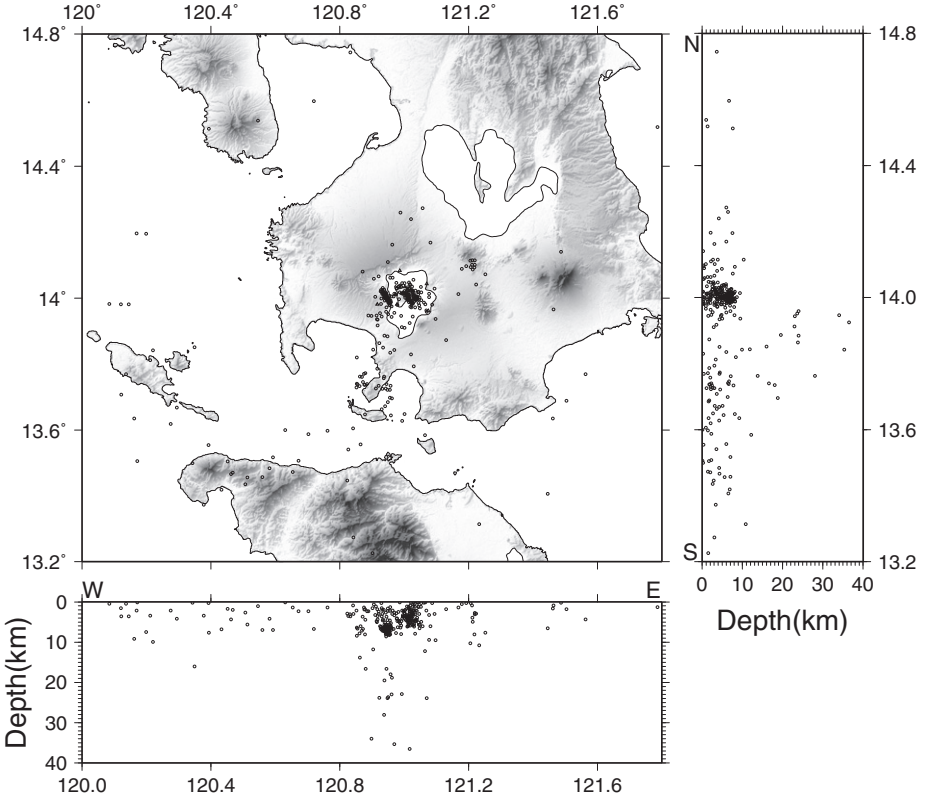

Fig. 8. Map of final hypocenter locations determined from the VELEST.

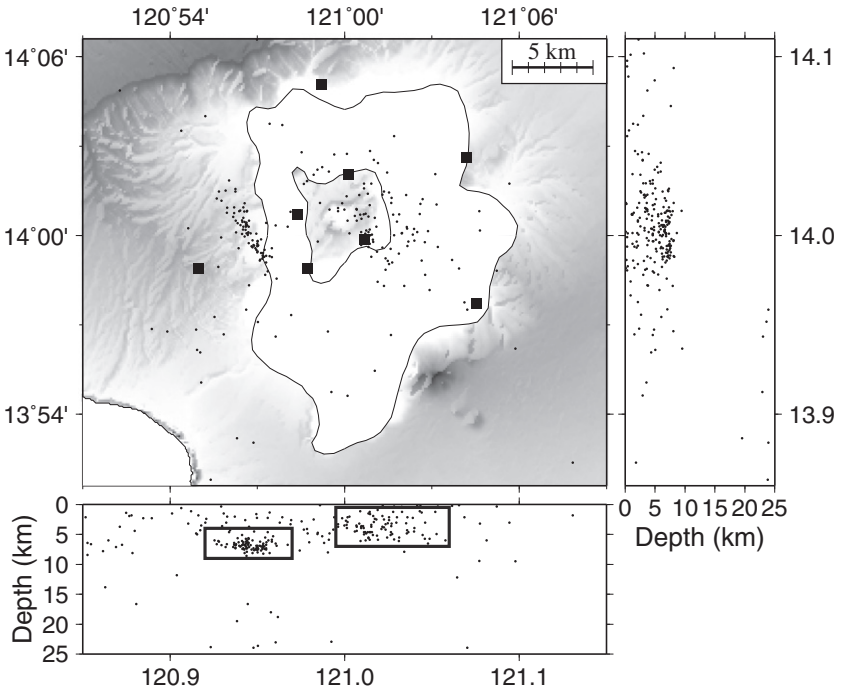

Fig. 9. Same as Fig. 8, while only the area near Taal Caldera is displayed for better illustration. Most events are located at depths shallower than ~8 km. Two major earthquake groups were noticed (marked by boxes) from the E–W section, with one clustering underneath the western shore of Taal lake, and the other spread around the eastern flank of Taal Volcano.

determined based on Wadati diagram (Kisslinger and Eengahl, 1973) (Fig. 5). Only events with root mean square (RMS) residuals less than 0.25 are used to derive the 'minimum 1-D velocity model' (Kissling, 1988). This criterion let to the rejection of about 2/3 of all events. The remaining qualified data set consists of 1391 P-wave and 973 S-wave arrivals recorded from 338 earthquakes.

The 'minimum 1-D velocity model' was proposed by Kissling (1988), who also developed the computer package VELEST (Kissling, 1995) to solve for the 'minimum 1-D velocity model' from a set of local earthquakes. It represents an ideal 1-D velocity model obtained by the damped least-square method that takes into account station corrections. For details on the methodology used in VELEST and processing procedure, the reader is referred to Kissling (1995).

The resulting model from the 14-layer starting model is shown in Fig. 6. The result suggests that velocity boundaries at 10 km, 14 km, 18 km and 20 km are not necessary. For the larger depths, from the facts that most events are shallow (<10 km), and there is only minor adjustment for depth below 25 km after the inversion, the boundary at 30 km is also removed in the updated starting model.

Using the updated 9-layer starting model, we start over the operation of VELEST. Both the starting model and the final model are displayed in Fig. 7, and are listed in Tables 4 and 5.

5. Spatial distribution of located earthquakes

The distribution of resulting earthquake locations are shown in Fig. 8. Except few deeper events in area around southern shore of the Taal Lake, most events occurred at shallow depth, and clustered beneath Taal Volcano, suggesting that they are likely induced by volcanic activities at this depth range.

The depth distribution these events may help us to better address the resolving ability of the derived 1-D model. Since all the events used in the inversion are distributed within the depth range from 0 to 40 km, most of them occurred at very shallow depths (<10 km), and only four events are located at depths deeper than 25 km. Therefore, it is expected that the average structure at shallow depths are better constrained, and resolution for depths below 25 km is less reliable.

A better illustration of seismicity underneath Taal Caldera is shown in Fig. 9. For this small area (~30 × 30 km), most events are located at depths shallower than ~8 km. Two major earthquake groups were noticed from the seismicity in the E–W section as indicated by two boxes in Fig. 9. Events in the group underneath the western shore of Taal lake are tightly clustered with a narrow depth range (~4–8 km), and their linear distribution indicates the probable presence of a subsurface fault. Events in the other group are less compact, and most of them are spread around the eastern flank of Taal Volcano.

Although there is no direct information about the locations for events documented earlier, it was reported that active fissures along the northern flank of the Taal Volcano opened during the 1992–1994 earthquake swarms, implying they are likely spatially correlated. On the other hand, during the 1965 eruption, the southwest flank was the place where pyroclastic surges originated. However, both the northern and southern flanks were seismically quiet during our observation period, implying that a spatial migration of magma activities may have occurred during this time period.

6. Conclusions

In this study we have developed a 9-layer 1-D model for Vp and Vs using carefully selected data from 338 local earthquakes recorded by a newly deployed seismic network in Taal Volcano. A novel technique of correcting time shifts in the internal clock that is based on noise-derived EGFs has been also introduced.

The reference 1-D model represents one step further towards more advanced seismic studies. Future objectives include an investigation of the spatio-temporal pattern of seismicity in Taal over time periods much larger than the one presented here. Of particular importance is the identification of volcanoseismic signals,

generated by fluid transfer processes, such as low/mixed frequency events and possibly volcanic tremor. Further analysis of these signals in terms of location and source properties is likely to shed light on how the magmatic system beneath Taal works and also help towards volcanic hazard assessment. Finally, as more data accumulate it will be possible to use local earthquake tomography in order to investigate the 3D velocity structure of the volcano and pinpoint any locations of partial melt.

Acknowledgements

We would like to thank the Philippine Institute of Volcanology and Seismology (PHIVOLCS) for their assistance in the deployment and maintenance of the seismic network. This research is supported by the National Science Council of Taiwan under the grants NSC 100-2116-M-002-025 and NSC 100-2119-M-001-020.

References

Bartel, B.A., Hambuger, M.W., Meertens, C.M., Lowry, A.R., Corpuz, E., 2003. Dynamics of active magmatic and hydrothermal systems at Taal Volcano, Philippines, from continuous GPS measurements. Journal of Geophysical Research 108 (B10), 2475. http://dx.doi.org/10.1029/2002JB002194.

Bryan, C.J., Sherburn, S., 1999. Seismicity associated with the 1995–1996 eruptions of Ruapehu Volcano, New Zealand: narrative and insights into physical process. Journal of Volcanology and Geothermal Research 90, 1–18. http://dx.doi.org/10.1016/S0377-0273(99)00016-5.

Brenguier, F., Shapiro, N.M., Campillo, M., Ferrazzini, V., Duputel, Z., Coutant, O., Nercessian, A., 2008. Towards forecasting volcanic eruptions using seismic noise. Nature 1, 126–130. http://dx.doi.org/10.1038/ngeo104.

Chouet, B.A., 1996. Long-period volcano seismicity: its source and use in eruption forecasting. Nature 380, 309–316.

Harlow, D.H., Laguerta, J.A., Power, Laguerta, E.P., Ambubuyog, G., White, R.A., Hoblitt, R.P., 1996. Precursory seismicity and forecasting of the June 15, 1991, eruption of Mount Pinatubo. In: Punongbayan, R.S., Newhall, C.G. (Eds.), Fire and Mud Eruptions and Lahars of Mount Pinatubo, Philippine. University of Washington Press, Seattle.

Jones, J.P., Thurber, C.H., Lutter, W.J., 2001. High precision location of pre-eruption seismicity at Mount Pinatubo, Philippines, 30 May–3 June, 1991. Physics of the Earth and Planetary Interiors 123, 221–232. http://dx.doi.org/10.1016/s0031-0201(00)00211-9.

Kennett, B.L.N., Engdahl, E.R., Buland, R., 1995. Constraints on seismic velocities in the Earth from travel times. Geophysical Journal International 122, 108–124.

Kisslinger, Carl., Eengahl, E.R., 1973. The interpretation of the Wadati diagram with relaxed assumptions. Bulletin of the Seismological Society of America 63, 1723–1736.

Kissling, E., 1988. Geotomography with local earthquake data. Reviews of Geophysics 26, 659–698.

Kissling, E., 1995. Velest Users Guide, International report Institute of Geophysics, ETH Zurich.

Kumagai, H., Chouet, B.A., Nakano, M., 2002. Temporal evolution of a hydrothermal system in Kusatsu-Shirane Volcano, Japan, inferred from the complex frequencies of long-period events. Journal of Geophysical Research 107 (B10), 2236. http://dx.doi.org/10.1029/2001JB000653.

Konstantinou, K.I., Lin, C.-H., Liang, W.-T., 2007. Seismicity characteristics of a potentially active quaternary volcano: the Tatun Volcano Group, northern Taiwan. Journal of Volcanology and Geothermal Research 160, 300–318. http://dx.doi.org/10.1016/j.jvolgeores. 2006.09.009.

Lee, W.H.K., Lahr, J.C., 1972. Hypo71: a computer program for determining hypocenter, magnitude, and fist motion pattern for local earthquakes. Open File Report 75–311, US Geological Survey.

Lukac, M., Davis, P., Claytion, R., Estrin, D., 2009. Recovering temporal integrity with data driven time synchronization. In: Proceedings of the 2009 International Conference on Information Processing in Sensor Networks 00. pp. 61–72.

McNutt, S.R., 1996. Seismic monitoring and eruption forecasting of volcanoes: a review of the state-of-the-art and case histories. In: Scarpa, Tilling (Ed.), Monitoring and Mitigation of Volcanic Hazards. Springer-Verlag, Berlin.

Moore, J.G., Nakamura, K., Alcaraz, A., 1966. The 1965 eruption of Taal Volcano. Science 151, 955–960.

Shapiro, N.M., Campillo, M., 2004. Emergence of broadband Rayleigh waves from correlations of the ambient seismic noise. Geophysical Research Letters 31, L07614. http://dx.doi.org/10.1029/2004GL019491.

Sherburn, S., Scott, B.J., Nishi, Y., Sugihara, M., 1998. Seismicity at White Island Volcano, New Zealand: a revised classification and inferences about source mechanism. Journal of Volcanology and Geothermal Research 83, 287–312.

Snieder, R., 2004. Extracting the Green's function from the correlation of coda waves: a derivation based on stationary phase. Physical Review E 69, 046610. http://dx.doi.org/10.1103/PhysRevE.69.046610.

Tanaka, S., Hamaguchi, H., Ueki, S., Sato, M., Nakamichi, H., 2002. Migration of seismic activity during the 1998 volcanic unrest at Iwate Volcano, Northeastern Japan, with reference to P and S wave velocity anomaly and crustal deformation. Journal of Volcanology and Geothermal Research 113, 399–414. http://dx.doi.org/10.1016/S0377-0273(01)00273-6.

Weaver, R.L., Lobkis, O.I., 2001. Ultrasonics without a source. Thermal fluctuation correlations at MHz frequencies. Physical Review Letters 87, 134301. http://dx.doi.org/10.1103/PhysRevLett.87.134301.

You, S.-H., Gung, Y., Chiao, L.-Y., Chen, Y.-N., Lin, C.-H., Liang, W.-T., Chen, Y.-L., 2010. Multi-scale ambient noise tomography of short period rayleigh waves across Northern Taiwan. Bulletin of the Seismological Society of America 100, 3165–3173. http://dx.doi.org.10.1785/0120090394.

Zlotnicki, J., Sasai, Y., Toutain, J.P., Villacorte, E.U., Bernard, A., Julio, P.S., Gordon Jr., J.M., Corpuz, E.G., Harada, M., Punongbayan, J.T., Hase, H., Nagao, T., 2009. Combined electromagnetic geochemical and thermal surveys of Taal Volcano (Philippines) during the period 2005–2006. Bulletin of Volcanology 71, 29–47. http://dx.doi.org/10.1007/s00445-008-0205-2.